Biophysical Journal Volume 77 November 1999 2648–2656

Supramolecular Structures of Peptide Assemblies in Membranes by Neutron Off-Plane Scattering: Method of Analysis

Lin Yang, Thomas M. Weiss, Thad A. Harroun, William T. Heller, and Huey W. Huang
Physics Department, Rice University, Houston, Texas 77251-1892 USA

ABSTRACT In a previous paper (Yang et al., *Biophys. J.* 75:641–645, 1998), we showed a simple, efficient method of recording the diffraction patterns of supramolecular peptide assemblies in membranes where the samples were prepared in the form of oriented multilayers. Here we develop a method of analysis based on the diffraction theory of two-dimensional liquids. Gramicidin was used as a prototype model because its pore structure in membrane in known. At full hydration, the diffraction patterns of alamethicin and magainin are similar to gramicidin except in the scale of q (the momentum transfer of scattering), clearly indicating that both alamethicin and magainin form pores in membranes but of different sizes. When the hydration of the multilayer samples was decreased while the bilayers were still fluid, the in-plane positions of the membrane pores became correlated from one bilayer to the next. We believe that this is a new manifestation of the hydration force. The effect is most prominent in magainin patterns, which are used to demonstrate the method of analysis. When magainin samples were further dehydrated or cooled, the liquid-like diffraction turned into crystal-like patterns. This discovery points to the possibility of investigating the supramolecular structures with high-order diffraction.

INTRODUCTION

It has long been speculated that membrane active peptides may self-assemble into supramolecular structures within fluid membranes. The best known example is alamethicin. Both its crystalline structure (Fox and Richards, 1982) and its single-channel conduction behaviors (Bauman and Mueller, 1974; Latorre and Alvarez, 1981) suggested that alamethicin monomers assemble in the barrel-stave fashion to form transmembrane pores. Other peptides, such as melittin and magainin, are also likely to form pores in lipid bilayers as suggested by ion conduction (Tosteson and Tosteson, 1981; Duclohier et al., 1989; Juretic et al., 1994), leakage experiments (Matsuzaki et al., 1996, 1997; Ladokhin, 1997), and other evidence (Dufourcq et al., 1986). However, there has not been an experimental method capable of directly observing such oligomeric peptide structures in membranes. A few years ago we successfully detected membrane pores with neutron in-plane scattering (He et al., 1995). Neutron detects structures within the membrane where the neutron scattering-length densities are different from that of a pure lipid bilayer. In particular, use of D_2O makes water-filled pores within the membrane stand out against the lipid background. (In contrast, peptide pores in fluid membranes, with the exception of gramicidin, are difficult to detect by x-ray.) This method allowed us to detect and measure the size of the alamethicin and magainin pores (He et al., 1995, 1996; Ludtke et al., 1996).

However, to fully characterize these supramolecular structures in membranes, the diffraction data must cover all the reciprocal space, including the momentum transfer **q** projected out-of-plane as well as in-plane. Normally, diffraction measurement in a two-dimensional q space is a time-consuming process. In a previous paper (Yang et al., 1998), we showed a simple method of recording the complete pattern using existing small-angle neutron scattering facilities. By this method, a complete diffraction pattern of a typical peptide-in-membrane sample can be obtained within one hour at the Cold Neutron Research Facility of the National Institute of Standards and Technology (Gaithersburg, MD). In this paper, we present the method for analyzing such diffraction patterns.

When multilayers of membranes are fully hydrated, the individual bilayers are well separated by intercalating water layers, so that the in-pane positions of embedded objects, such as membrane pores, are uncorrelated between bilayers. In such cases, the q_z (the out-of-plane **q** component) dependence of the scattering pattern is governed solely by the form factor of the scattering objects. The structural information for the lateral organization can be obtained by in-plane scattering, as we have shown previously (He et al., 1995, 1996; Ludtke et al., 1996). However, some of the most intriguing phenomena of peptide-membrane interactions manifest themselves in less than fully hydrated conditions. In many cases, when the multilayer samples were underhydrated, the diffraction patterns showed that the in-plane positions of pores became correlated between bilayers. This indicated a lateral repulsion between pores residing in neighboring bilayers. This phenomenon of lateral force between embedded objects in two neighboring bilayers has not been observed before. In very low hydrations or low temperature, strong correlations order the pores into a quasicrystalline, thereby allowing for the possibility of investigating the supramolecular structures with high-order diffraction.

Received for publication 11 May 1999 and in final form 29 July 1999.
Address reprint requests to Dr. Huey W. Huang, Physics Department, Rice University, Houston, TX 77251-1892. Tel.: 713-527-4899; Fax: 713-527-9033; E-mail: huang@ion.rice.edu.

0006-3495/99/11/2648/09 $2.00

X-RAY EXPERIMENT

The neutron data we will analyze here were measured at the National Institute of Standards and Technology, by the method reported in Yang et al. (1998). The data include alamethicin in dilauroyl phosphatidylcholine (DLPC), and magainin in DLPC, in dimyristoyl phosphatidylcholine (DMPC), and in the 3:1 mixture of DMPC and dimyristoyl phosphatidylglycerol (DMPG).

In addition, we performed x-ray experiments using the same scattering geometry as the neutron experiment described in Yang et al. (1998). A point source of Cu K_α radiation (operating at 35 mA/40 kV) was used. A thin Ni filter was placed at the tube exit to remove most of the Cu K_β radiation. The beam was then focused by a pair of spherically bent x-ray mirrors (Charles Supper Co., Natick, MA). The mirrors were Ni-coated to further reduce the amount of K_β radiation. The multilamellar sample, oriented at an angle ω relative to the incident beam (Yang et al., 1998), was housed in a sealed chamber wherein the sample temperature and relative humidity of the air could be controlled. A small beamstop was placed directly behind the chamber to prevent excessive air scattering.

X-ray data were collected using a Siemens X1000 multiwire proportional chamber (512×512 pixel; Bruker AXS Inc., Madison, WI) at the sample-to-detector distance of 21.54 cm. The distance was measured using sucrose powder as a calibration standard. Data collection time ranged from 2 to 5 h, depending on the amount and quality of the sample.

DLPC was purchased from Avanti Polar Lipids (Alabaster, AL). Gramicidin D and thallium acetate (99.99% purity) were purchased from Sigma Chemical Co. (St. Louis, MO). All chemicals were used without further purification. Thallium acetate was added to the gramicidin sample to enhance the contrast of the gramicidin D channels (Olah et al., 1991; He et al., 1993a). Preparation for the gramicidin sample was the same as described previously (Olah et al., 1991; He et al., 1993a). Approximately 4–6 mg of hydrated sample was sandwiched between two polished and SiO_2-coated beryllium plates (0.5×15 mm diameter). The sample was thoroughly aligned to remove most of the smectic defects (Huang and Olah, 1987). For the measurement of pure lipid background, ~1 mg of DLPC was deposited from organic solvent (Ludtke et al., 1995) onto a thoroughly cleaned 0.2-mm-thick microscope cover glass. The organic solvent was removed by vacuum and the lipid was rehydrated with water vapor.

THEORETICAL ANALYSIS

Background-diffraction patterns of pure lipid bilayers

One expects perfectly aligned lipid multilayers to produce Bragg peaks at $q_z = n(2\pi/d)$ ($n = 1, 2, 3, \ldots$) and $q_r = 0$, where q_z and q_r are the projections of the momentum transfer of neutron or x-ray scattering perpendicular and parallel to the plane of bilayers, respectively, and d is the repeat spacing of the multilayers. d is typically about 60 Å, so the Bragg peaks are located at $q_z \sim 0.1, 0.2, \ldots,$ Å^{-1}. In addition, along the plane of the bilayer, the hydrocarbon chains give rise to the so-called paraffin peak at $q_r \sim 2\pi/(4.6$ Å$) \sim 1.4$ Å^{-1} (He et al., 1993a). However, in real samples of membrane multilayers, the Bragg peaks often extend into rings $(q_z^2 + q_r^2)^{1/2} = n(2\pi/d)$, as will be explained below. We need to be concerned with the first two of these rings because they are in the background of the peptide patterns, which lie typically in the range of $|\mathbf{q}| \sim$ 0.01–0.2 Å^{-1}. The paraffin peak is outside the range of interest here.

Figure 1 shows an example of diffraction pattern by pure DLPC multilayers. The pattern was measured by the method of off-plane scattering (Yang et al., 1998) with the multilayer sample oriented at $\omega = (90° -$ the Bragg angle). Two rings corresponding to the first and the second Bragg orders are visible. Such rings are the result of two effects: the broadening of the Bragg peaks and the presence of smectic defects in multilayers. First, we discuss the effect of peak broadening that could be caused by instrumental resolution or by sample imperfection. The instrument factors include the energy and momentum resolutions of the beam and the detector. In particular, if a small angle neutron scattering facility is used, the energy resolution of the incident beam is usually the dominant instrument factor, because the wavelength resolution ($\Delta\lambda/\lambda$) could be as large as 30%. On the contrary, x-ray facilities, whether an x-ray generator or synchrotron, usually have excellent energy resolutions ($\Delta E/E < 10^{-3}$). Momentum (or angular) resolutions of either neutron or x-ray facilities are usually not a factor compared to the broadening effect due to either neutron energy resolution or sample imperfection. The qualities of the sample that might contribute to peak broadening include sample mosaic spread, domain size (Warren, 1969), and undulation fluctuations (Caillé, 1972) of the bilayer plane. All of these factors are well understood. The effect of undulation is important only when the sample is fully or over hydrated.

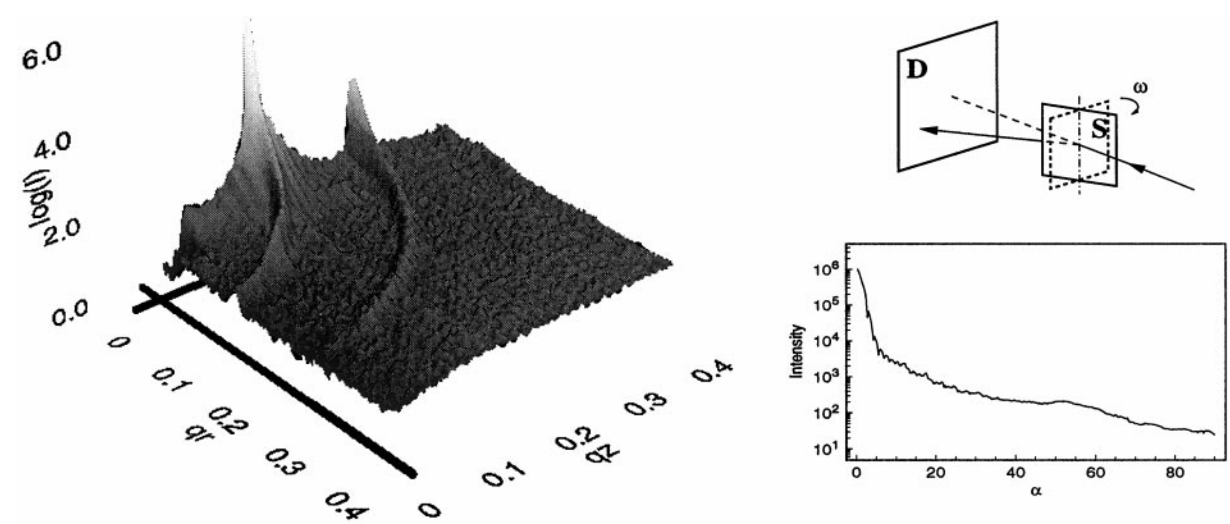

FIGURE 1 (*Left*) Diffraction pattern of DLPC multilayers deposited on a glass substrate from organic solvent. Two rings corresponding to the first and the second Bragg orders are visible. The unit of q is Å^{-1}. (*Right Top*) The geometry of off-plane scattering. S represents the plane of multilamellar membranes; it is rotated by an angle ω about the vertical axis from parallel to the detector D. The pattern shown here was measured at $\omega = (90° -$ the Bragg angle). (*Right Bottom*) The intensity of the first Bragg ring is plotted as a function of α, the angular coordinate of the ring defined as 0° along q_z and 90° along q_r.

The sample producing Fig. 1 was equilibrated at ~95% relative humidity (RH) and the diffraction was measured by x-ray. In this case, the broadening of the Bragg peaks was dominated by the effect of sample mosaics. (A poorly aligned sample was chosen for the purpose of illustration.) Consider the first-order ring, and let us specify its angular coordinate α to be 0° along the q_z axis, increasing to 90° along the q_r axis or the equator. The intensity of the ring peaks at $\alpha = 0°$, and decreases rapidly by two orders of magnitude when it reaches $\alpha \sim 5°$. This part of the ring is roughly Gaussion and can be attributed to the sample mosaic spread (Warren, 1969). The reason the diffraction ring extends to the equator is that there were misaligned defects in the sample. (The intensity from 50° to 90° was distorted by the complicated effects of sample edge and substrate absorption—effects that are not as important in neutron diffraction.) Because the mosaic spread and the amount of defect vary from sample to sample, the intensity of these Bragg rings varies from very strong to invisible (see He et al., 1996 for the description and control of smectic defects in multilayer samples). When these rings appear as part of the diffraction pattern produced by a peptide sample, they are generally recognizable and, in most cases, separable from the peptide patterns.

Scattering theory of fluid multilayers

The coherent neutron scattering intensity $I(\mathbf{q})$ is given by (Bacon, 1975)

$$I(\mathbf{q}) = \langle |A(\mathbf{q})|^2 \rangle = \left\langle \left| \int \rho(\mathbf{R}) \exp(i\mathbf{q} \cdot \mathbf{R})\, d\mathbf{R} \right|^2 \right\rangle, \tag{1}$$

where $A(\mathbf{q})$ is the scattering amplitude and $\rho(\mathbf{R})$ is the scattering-length density at the position $\mathbf{R}$ in the sample. Assuming that identical channels (pores) are embedded in a stack of planar lipid bilayers all aligned parallel to the x–y plane, we write $\rho(\mathbf{R})$ as $\rho_o(\mathbf{R}) + \phi(\mathbf{R})$, where $\rho_o(\mathbf{R})$ represents the scattering-length density of pure lipid multilayers (including the intercalating water layers) without peptides, and $\phi(\mathbf{R})$ represents the scattering-length contrast of the channels against the lipid background. Defining the scattering amplitudes

$$A_o(\mathbf{q})) = \int \rho_o(\mathbf{R}) \exp(i\mathbf{q} \cdot \mathbf{R})\, d\mathbf{R}$$

and

$$A_\phi(\mathbf{q})) = \int \phi(\mathbf{R}) \exp(i\mathbf{q} \cdot \mathbf{R})\, d\mathbf{R},$$

we have

$$I = \langle |A_o + A_\phi|^2 \rangle = \langle |A_o|^2 + |A_\phi|^2 + 2\,\mathrm{Re}(A_o A_\phi^*) \rangle. \tag{2}$$

The contribution of $A_o(\mathbf{q})$ is described in the last section. We will assume that $A_o(\mathbf{q})$ and $A_\phi(\mathbf{q})$ are separable and concern ourselves with the scattering by $\phi(\mathbf{R})$ alone. We denote the positions of the centers of the channels by R_n, $n = 1, 2, \ldots, N$. It is convenient to write $\phi(\mathbf{R}) = \Sigma_n\, \phi_c(\mathbf{R} - \mathbf{R}_n)$, where $\phi_c(\mathbf{R} - \mathbf{R}_n)$ is the scattering-length contrast of a channel, centered at $\mathbf{R}_n$, against the lipid background. It follows that

$$\begin{aligned} I &= \left\langle \left| \int \phi(\mathbf{R}) \exp(i\mathbf{q} \cdot \mathbf{R})\, d\mathbf{R} \right|^2 \right\rangle \\ &= \left| \int \phi_c(\mathbf{R}) \exp(i\mathbf{q} \cdot \mathbf{R})\, d\mathbf{R} \right|^2 \left\langle \left| \sum_n \exp(i\mathbf{q} \cdot \mathbf{R}_n) \right|^2 \right\rangle. \end{aligned} \tag{3}$$

The scattering amplitude by an individual channel (pore) is called the form factor $F_\phi(q_z, q_r) = \int \phi_c(\mathbf{r}) \exp(i\mathbf{q} \cdot \mathbf{R})\, d\mathbf{R}$. The second factor on the right-hand side of Eq. 3, $\langle |\Sigma_n \exp(i\mathbf{q} \cdot \mathbf{R}_n)|^2 \rangle$, is written as the product of N, the number of channels, and the structure factor $S(q_z, q_r)$, so the scattering intensity is given in the conventional form (Bacon, 1975; Warren, 1969),

$$I(q_z, q_r) = N |F_\phi(q_z, q_r)|^2 S(q_z, q_r). \tag{4}$$

By the same method of developing the in-plane scattering theory (He et al., 1993a), the structure factor can be expressed as

$$S(q_z, q_r) = 1 + \sum_m e^{iq_z(z_m - z_o)} \int n_{0m}(\mathbf{r}) e^{i\mathbf{q}_r \cdot \mathbf{r}}\, d\mathbf{r}, \tag{5}$$

where $\mathbf{r}$ is the two-dimensional coordinate in the plane parallel to the membranes. The difference between the present theory and the in-plane scattering where only one bilayer was considered is that here, the in-plane positions of the scattering objects (the pores) may be correlated between different bilayers. The correlation function $n_{0m}(\mathbf{r})$ is defined as the average number of pores in the mth bilayer at position $\mathbf{r}$ relative to an arbitrarily chosen pore in the 0th bilayer. The z dependence is discrete: $z = md.$, $m = 0, \pm 1, \pm 2, \ldots$. Furthermore $n_{0m} = n_{0-m}$. Expanding the sum in Eq. 5 and making use of the fact that the distribution of pores in a fluid bilayer is isotropic in the plane, we have

$$S(q_z, q_r) = S_{00}(q_r) + 2\cos(q_z d) S_{01}(q_r) + \cdots, \tag{6}$$

$$S_{0m}(q_r) = \delta_{0m} + \int (n_{0m}(r) - \bar{n}) J_0(q_r r) 2\pi r\, dr, \tag{7}$$

where $\bar{n}$ is the average density of pores in each bilayer and J_0 is the 0th order Bessel function. S_{0m} are similar to the partial structure factors in a multicomponent liquid (Bacon, 1975). S_{00} is the in-plane structure factor, due to the correlations of the pores in the same bilayer. S_{01} is due to the correlations between the pores residing in nearest neighboring bilayers. Note that the q_z-dependence of $S(q_z, q_r)$ comes from the correlations between different bilayers. If there are no interbilayer correlations in the in-plane positions of the pores, that is, $S_{0m} = 0$ for all $m \neq 0$, then $S(q_z, q_r) = S_{00}(q_r)$, the structure factor has no q_z-dependence.

The contrast form factor $F_\phi(q_z, q_r)$ is given by

$$F_\phi(q_z, q_r) = F_p(q_z, q_r) - F_{lb}(q_z, q_r), \tag{8}$$

where $F_p(q_z, q_r)$ is the form factor of the pore and $F_{lb}(q_z, q_r)$ is the form factor of a patch of lipid bilayer filling the space of the pore. In neutron diffraction, the contrast form factor is dominated by the D_2O-filled water channel, approximated as a cylinder of diameter a and height b. a is a fitting parameter but b is the bilayer thickness. The q_z-dependence of a cylindrical form factor of height b is $\sin(q_z b/2)/(q_z b/2)$. Thus, for neutron diffraction, the q_z-dependence of $F_\phi(q_z, q_r) \approx \sin(q_z b/2)/(q_z b/2)$. For x-ray diffraction, the contribution of lipids can be significant. For gramicidin samples, the q_z-dependence of $F_\phi(q_z, q_r) = F_G(q_z) - F_{lb}(q_z)$. The q_z-dependence of the gramicidin form factor $F_G(q_z)$ can be calculated directly from the nuclear magnetic resonance (NMR) structure of the gramicidin channel (Arseniev et al., 1985; Nicholson and Cross, 1989). The q_z-dependence of a lipid bilayer $F_{lb}(q_z)$ is directly measurable by lamellar diffraction. For example, the x-ray form factor of the DLPC bilayer has been measured by Olah et al. (1991). The diffraction patterns we have observed divide into three cases.

Case 1: No interbilayer correlations

Diffraction patterns with no interbilayer correlations were observed when the multilayers were sufficiently hydrated. Figure 2 shows examples of three different peptides, gramicidin, alamethicin, and magainin, in fully hydrated DLPC bilayers. Gramicidin is included here as a prototype model, because it has a well-established channel structure. The 15-amino acid peptide forms a dimeric pore that has a cylindrically averaged outside

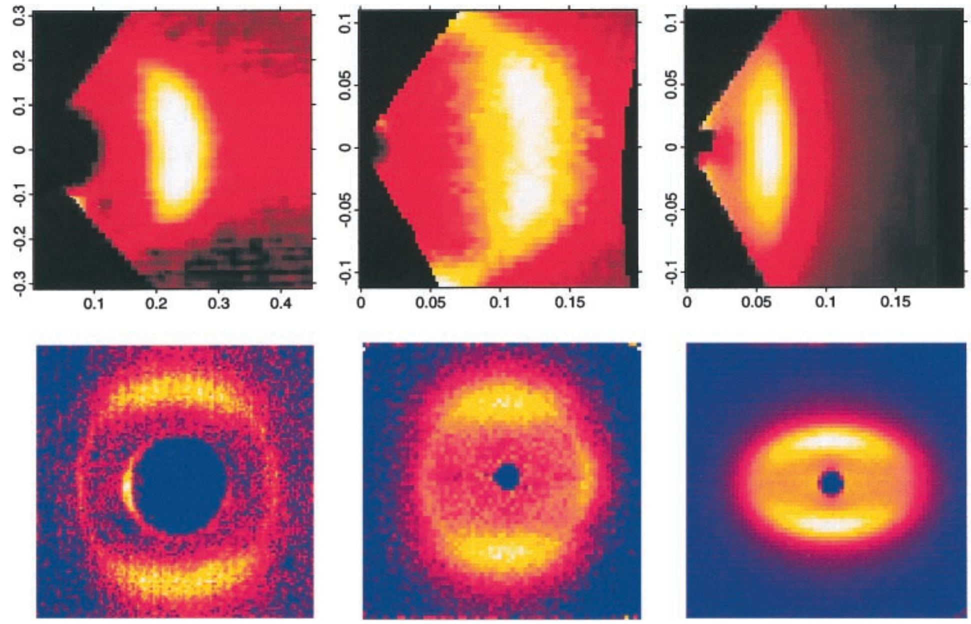

FIGURE 2 Diffraction patterns of three peptides in DLPC bilayers measured by the off-plane scattering method described in Yang et al. (1998). The multilayers were oriented at $\omega = 60°$ with respect to the detector. The bottom row shows the intensity patterns on the area detector and the top row shows the intensity patterns in the (q_z ordinate, q_r abscissa; unit $Å^{-1}$) space. (*Left column*) gramicidin in DLPC at the peptide-to-lipid molar ratio P/L = 1/10, by x-ray. (*Middle column*) alamethicin in DLPC at P/L = 1/30, by neutron with D_2O. (*Right column*) magainin in DLPC at P/L = 1/30, by neutron with D_2O. All samples were near full hydration. Note that all three patterns are similar to one another except in the scale of q.

diameter ~18 Å (Harroun et al., 1999a,b) and an inside pore of diameter ~4 Å (Arseniev et al., 1985; Nicholson and Cross, 1989). The diffraction of gramicidin channels can be observed with either x-ray or neutron. In fact, diffraction by x-ray provides a stronger contrast than by neutron because the gramicidin channel has a rigid peptide backbone (He et al., 1993a). In comparison, the peptide assemblies in the magainin and alamethicin pores are not rigid, so they do not provide a sufficient x-ray contrast against the lipid background, unless the samples crystallize (see below). In fluid membranes, the magainin and alamethicin pores have been observed only by neutron with the aid of D_2O hydration. All gramicidin patterns discussed in this paper were obtained by x-ray diffraction; all magainin and alamethicin patterns were by neutron with D_2O replacing the water.

The key observation here is that the q_z-dependence of these diffraction patterns (Fig. 2) is consistent with that of the form factor squared $|F_\phi(q_z, q_r)|^2$. This is displayed in Fig. 3 where the q_z-dependence of each diffraction pattern at the peak value of q_r is shown, to a large extent, in agreement with the q_z-dependence of $|F_\phi(q_z, q_r)|^2$. That means that, according to Eq. 4, the structure factor $S(q_z, q_r)$ has no significant q_z-dependence. According to Eqs. 5 and 6, $S(q_z, q_r)$ is essentially $S_{00}(q_r)$. All S_{0m}, $m \neq 0$ terms in the expansion of $S(q_z, q_r)$ (Eq. 6) vanish. The individual pores are positionally uncorrelated from one bilayer plane to the next. Because of the well-established pore structure of gramicidin, Fig. 2 (*left*) may be regarded as the representative diffraction pattern of pores in fluid membranes with no interbilayer correlations. Alamethicin and magainin produced similar patterns (Fig. 2, *middle* and *right*, respectively), so each peptide must have created pores in the lipid bilayers. Furthermore, from the position of the peak in q_r, one can roughly estimate the external size of the pores before a detailed analysis. It has been shown in the hard-core approximation that the position of the peak in q_r is roughly 7.0 (the first maximum of J_0) divided by the outside diameter of the pore, relatively insensitive to the pore density (Hansen and McDonald, 1986; He et al., 1993a,b). Therefore, roughly the external diameter of the magainin pore is twice the external diameter of the alamethicin pore, which is, in turn, twice the external diameter of the gramicidin channel.

When there are no interbilayer correlations, the q_r-dependence of the diffraction pattern can be taken directly from the in-plane ($q_z = 0$) scattering,

$$I(0, q_r) = N|F_\phi(0, q_r)|^2 S_{00}(q_r). \tag{9}$$

This justifies the previous use of in-plane scattering to study the gramicidin distribution in membranes (He et al., 1993a,b; Harroun et al., 1999a) and to analyze the alamethicin pore (He et al., 1995, 1996) and the magainin pore (Ludtke et al., 1996), where the samples were measured near full hydration. Eq. 9 is a typical scattering formula for a liquid (except that, here, it is in two dimensions) for which the methods of analysis are well known (Warren, 1969; Bacon, 1975; Hansen and McDonald, 1986). In the case of gramicidin, the form factor is known. The scattering curve can be

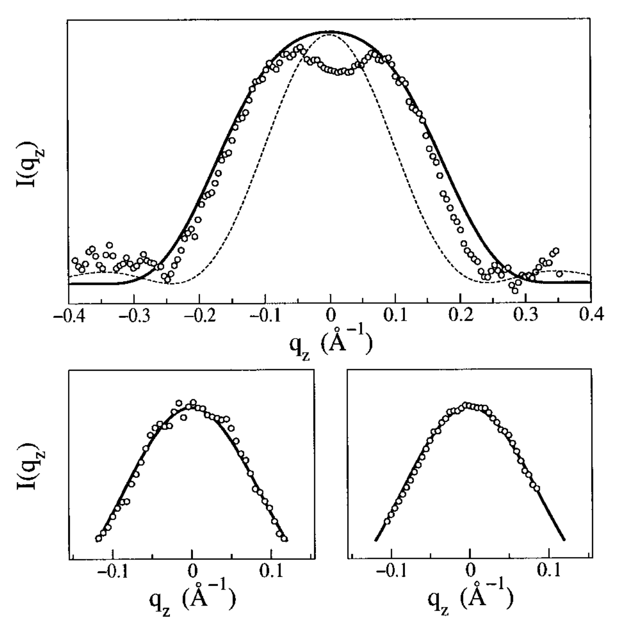

FIGURE 3 The q_z-dependence of the diffraction patterns shown in Fig. 2. The data (○) were taken along the q_z coordinate at q_r fixed at the maximum intensity of each pattern. (*Top*) gramicidin pattern. The dotted line is the form factor of the gramicidin channel $|F_G(q_z)|^2$. The solid line is the q_z-dependence of $|F_\phi(q_z, q_r)|^2 = |F_G(q_z) - F_{lb}(q_z)|^2$. The contribution of the lipid background is significant. The data show a small dip at the center ($q_z = 0$) indicating that the sample was not quite fully hydrated (see Fig. 4 for the hydration dependence). (*Bottom left and right*) alamethicin and magainin pattern, respectively. Both solid lines are $|\sin(q_z b/2)/(q_z b/2)|^2$ with b = 30 Å approximately the thickness of DLPC bilayer.

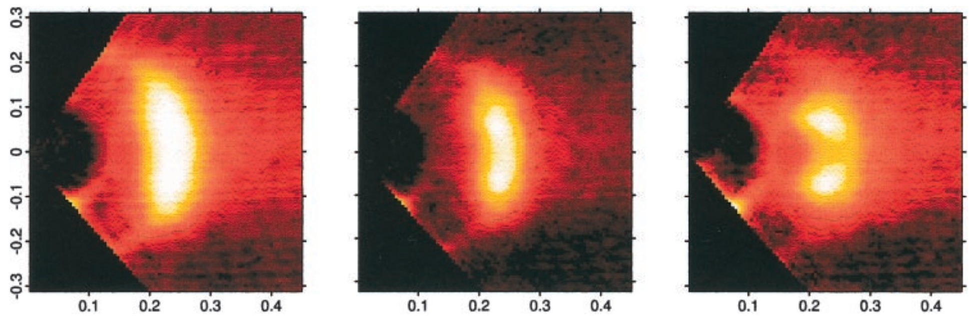

FIGURE 4 Diffraction patterns of one gramicidin sample at three hydration levels. (q_z ordinate, q_r abscissa; unit Å^{-1}) (*Left*) the same as shown in Fig. 2, the sample humidity was >95% RH. (*Middle*) ~90% RH. (*Right*) ~80% RH.

used to study, for example, the effect of membrane-mediated interactions on the distribution of the gramicidin channels in membranes (Harroun et al., 1999b). In the case of alamethicin and magainin, $F_\phi(0, q_r)$ is dominated by the D_2O column within the pore. The inside diameter of the pore is the dominating parameter in $F_\phi(0, q_r)$ (He et al., 1996). In contrast, $S_{00}(q_r)$ is most sensitive to the contact distance between two pores, that is equivalent to the outside diameter of the pores (He et al., 1993b). Thus in-plane scattering $I(0, q_r)$ provides accurate estimates for the inside and outside diameters of membrane pores. To narrow the uncertainties of the estimates, it is desirable to further restrict the model fitting by contrast variations. For example, we used deuterated lipids to obtain four independent in-plane scattering curves for alamethicin in DLPC bilayers, and demanded the same model (dominated by only two parameters, i.e., the inside and outside diameters) to agree with all the four curves (He et al., 1996).

The in-plane scattering curves of Fig. 2 (*left* and *middle*), had been analyzed previously in He et al. (1993a) and in He et al. (1996), respectively. The analysis of Fig. 2 (*right*) showed that the magainin pores in DLPC bilayers have an inside radius (the water channel) ~25 Å and an external radius ~42 Å. In comparison, the alamethicin pore in DLPC has an insider radius ~9 Å and an external radius ~20 Å (He et al., 1996). As mentioned above, the NMR structure of the gramicidin channel has an inside radius ~2 Å and an external radius ~9 Å.

Case 2: Weak interbilayer correlations

Partial structure factor S_{01}

When the q_z-dependence of the diffraction pattern deviates from that of $|F_\phi(q_z, q_r)|^2$, it implies that the structure factor $S(q_z, q_r)$ has significant q_z-dependence. It is clear from the expansion in Eq. 6 that some S_{0m}, $m \neq 0$ terms must contribute to $S(q_z, q_r)$. This means that individual pores are positionally correlated from one bilayer plane to the next. Diffraction patterns manifest interbilayer correlations when the multilayer samples were less than fully hydrated. Figure 4 shows patterns of one gramicidin sample in three different hydration levels. When the sample was highly hydrated, the q_z-dependence is maximum at $q_z = 0$. However, upon dehydration, the maximum intensity shifts off the equator, apparently deviating from the q_z-dependence of $|F_\phi(q_z, q_r)|^2$. The strength of interbilayer correlation at a given hydration level varies greatly with sample, depending on both the peptide and lipid composition. For example, magainin pores showed stronger interbilayer correlations than did alamethicin pores in both DLPC and DMPC. For both peptides, the degree of correlations was stronger in DMPC than in DLPC at the same level of dehydration. Like gramicidin, magainin patterns showed increasing interbilayer correlations with decreasing hydration (see an example shown under Case 3, below). All the effects of dehydration were reversible. When a dehydrated sample was rehydrated, the interbilayer correlations decreased. More systematic studies on hydration and dehydration are in progress.

When the interbilayer correlations are weak (to be justified below), we expect the structure factor to be dominated by the first two terms in the expansion shown in Eq. 6, which we will now use to analyze the example of magainin pores in DMPC/DMPG (3:1) bilayers measured at ~95% RH, shown in Fig. 5. This example is chosen because its corresponding in-plane scattering curve near full hydration has been analyzed earlier (Ludtke et al., 1996). If the truncated form of Eq. 6 is valid, depending on the sign of S_{00} and S_{01}, the maximum of the q_z-dependence can only occur at either $\cos(q_z d) = 1$ ($q_z = 0$) or $\cos(q_z d) = -1$ ($q_z = \pm\pi/d$). The pattern of Fig. 5 is consistent with the maxima being at $q_z = \pm\pi/d$. ($+q_z$ and $-q_z$ are symmetric.) This justifies the truncation of the expansion in Eq. 6 and keeping only two terms in the structure factor $S(q_z, q_r)$.

Assume that the q_z- and q_r-dependence of $F_\phi(q_z, q_r)$ can be factorized,

$$F_\phi(q_z, q_r) = \left[\frac{\sin(q_z b/2)}{q_z b/2}\right] F_\phi(0, q_r), \tag{10}$$

which is valid if the shape of the pore is cylindrical. We obtain

$$\frac{I(q_z, q_r)}{[\sin(q_z b/2)/(q_z b/2)]^2} = N|F_\phi(0, q_r)|^2[S_{00}(q_r) + 2\cos(q_z d)S_{01}(q_r)]. \tag{11}$$

The two scattering curves at $q_z = 0$ and at $q_z = \pm\pi/d$ are $N|F_\phi(0, q_r)|^2[S_{00}(q_r) \pm 2S_{01}(q_r)]$, from which we recover Eq. 9, $I_{00}(0, q_r) = N|F_\phi(0, q_r)|^2 S_{00}(q_r)$, and obtain a new equation,

$$I_{01}(0, q_r) = N|F_\phi(0, q_r)|^2 S_{01}(q_r). \tag{12}$$

Eq. 9 can also be obtained from Eq. 11 by choosing $q_z = \pm\pi/2d$. I_{00} and I_{01} were extracted from Fig. 5 using $b = 35.5$ Å and $d = 49.3$ Å (Harroun et al., 1999a) and shown in Fig. 6. I_{00} at 95% RH is nearly the same as the in-plane scattering curve measured near full hydration and analyzed previously (Fig. 4 of Ludtke et al., 1996). In contrast, I_{01} describes a phenomenon never measured before, that is, interactions of membrane-embedded objects between two lipid bilayers.

To extract the partial structure factor S_{01} from the data, we first analyzed I_{00} by the method of in-plane scattering (Ludtke et al., 1996). Because, by definition, the function $S_{00}(q_r)$ asymptotically levels to one at large q_r, one

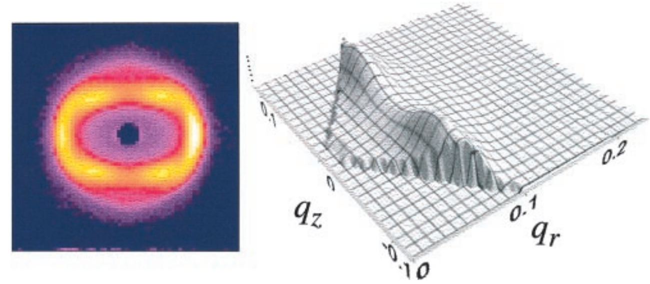

FIGURE 5 Diffraction pattern of magainin in DMPC/DMPG (3:1) at peptide-to-lipid molar ratio 1/30, 35°C and ~95% RH, measured by neutron with D_2O at $\omega = 60°$ (Yang et al., 1998). (*Left*) the intensity pattern on the area detector. (*Right*) the intensity pattern in the (q_z, q_r; unit Å^{-1}) space.

can normalize $I_{00}(0, q_r)$ by a constant multiplication factor, such that $I_{00}(0, q_r)$ fits $|F_\phi(0, q_r)|^2$ in the large q_r region (for details see He et al., 1993a, 1996). This same multiplication factor was then used to normalize $I_{01}(0, q_r)$—this process is equivalent to putting $N = 1$ in Eq. 9 and Eq. 12. $S_{01}(q_r)$ was then obtained by dividing the normalized $I_{01}(0, q_r)$ by the $|F_\phi(0, q_r)|^2$ obtained from the in-plane scattering analysis. The results are shown in Fig. 6. The correlation function $n_{01}(r)$ was obtained by a reverse Bessel transform on Eq. 7. Here r is the horizontal distance between a pore in the $m = 0$ bilayer and another pore in the $m = 1$ bilayer. This experimental $n_{01}(r)$ shows that, if there is a pore located at the origin in the $m = 0$ bilayer, the possibility of finding a pore near the origin of the $m = \pm 1$ bilayer is very small. Instead, there is a relatively high possibility of finding pores at $r \sim 46$ Å in the $m = \pm 1$ bilayer. For a qualitative understanding, one can compare the experimental $n_{01}(r)$ with the theoretical $n_{00}(r)$ obtained from the hard disk model (Fig. 6) where pores are freely diffusing in the same bilayer except that they are not allowed to overlap. The model $n_{00}(r)$ shows that, if there is a pore at the origin, then within the diameter A of the pore, the probability of finding another pore is zero ($n_{00}(r) = 0$ from $r = 0$ to A), but there is a relatively high possibility of finding pores right outside the excluded region. The experimental $n_{01}(r)$ has qualitatively the same features, indicating that the observed interbilayer correlations were caused by a horizontal repulsion between the pores residing in adjacent bilayers.

Analysis of partial structure factor S_{01}

The physics of the partial structure factor S_{01} is similar to that of a binary liquid, say, of atom A and B (Page and Mika, 1971). The function n_{00}, describing correlations between the pores in the same bilayer, is analogous to the correlation function between like atoms A–A, or B–B. The function n_{01}, describing correlations between the pores in one bilayer and the pores in the neighboring bilayer, is analogous to the correlation function between atoms A and atoms B. There is self-correlation in S_{00}, but there is no self-correlation in S_{01} (note the absence of one in the first term of Eq. 7 when $m \neq 0$). Indeed, an upside down bell-shaped S_{AB}, qualitatively similar to the experimental S_{01} shown in Fig. 6, was observed by neutron diffraction of liquid CuCl (Page and Mika, 1971).

We analyzed the S_{01} shown in Fig. 6 by a computer simulation. We used a model system of 20 bilayers with 120 pores in each bilayer, so the total number of pores is $N = 2400$. Each pore was represented by a disk of diameter A. The total area of each bilayer is such that the fraction of the area occupied by the disks is c. The value for c, 45%, was determined by the analysis of in-plane scattering (see Ludtke et al., 1996 for the discussion of c relative to the peptide/lipid ratio). Within the same bilayer, the disks diffuse around without restriction except that disks were not allowed to overlap with one another—we call this the hard disk condition. The value of A, 70 Å, was previously determined by the analysis of in-plane scattering (Ludtke et al., 1996). For simplicity, we assume a linear repulsive potential $V(r)$ as a function of the horizontal distance r between one pore in bilayer m and another pore in bilayer $m + 1$, with two parameters: the height U_0 and the range A_1, as shown in Fig. 6. The energy V was expressed in the unit of thermal energy k_BT (k_B being the Boltzmann constant and T the absolute temperature). To determine the distribution of the pores in each layer, we used the following Monte Carlo simulations. Each disk (pore) was allowed to move in its own layer only. Periodic boundary conditions were applied to each layer (i.e., if a pore moved out of its bilayer from the left edge, it would reenter the bilayer on the right edge), and to the stack of the layers (i.e., bilayer 1 is the same as bilayer 21). The system evolved by steps. In each step, each disk was, in turn, allowed to attempt an (in-plane) move of distance s in an arbitrarily chosen direction. For each move, the resulted energy change ΔE was calculated according to the potential energy specified above. A random number f

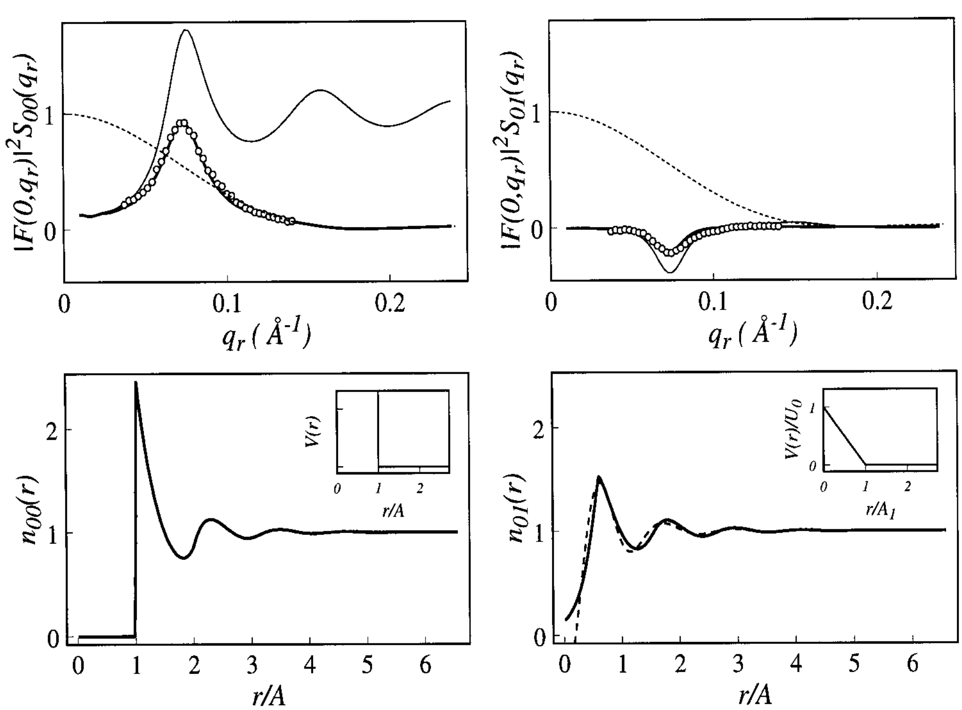

FIGURE 6 (*Top row*) The data (○) are $|F_\phi(0, q_r)|^2S_{00}(q_r)$ and $|F_\phi(0, q_r)|^2S_{01}(q_r)$ deduced from Fig. 5 as described in the text. (*Top left*) Data analysis for $|F_\phi(0, q_r)|^2S_{00}(q_r)$ has been described in Ludtke et al. (1996). The dotted line is $|F_\phi(0, q_r)|^2$. The thin solid line is $S_{00}(q_r)$ obtained by Eq. 7 from the simulated $n_{00}(r)$ shown in the bottom left panel, where the inset shows the interaction potential between the pores in the same bilayer. The thick solid line is the simulated $|F_\phi(0, q_r)|^2S_{00}(q_r)$. (*Top right*) The dotted line is the same $|F_\phi(0, q_r)|^2$ shown in the top left panel. The data $|F_\phi(0, q_r)|^2S_{01}(q_r)$ was divided by $|F_\phi(0, q_r)|^2$ and transformed by Eq. 7 to the experimental $n_{01}(r)$ shown as the dash line in the bottom right panel. The thin solid line is $S_{01}(q_r)$ obtained from the simulated $n_{01}(r)$ shown in the bottom right panel. The thick solid line (barely visible) is the simulated $|F_\phi(0, q_r)|^2S_{01}(q_r)$. (*Bottom right*) The dash line is the experimental $n_{01}(r)$. The solid line is the simulated $n_{01}(r)$. The inset shows the interaction potential between pores residing in two adjacent bilayers.

between 0 and 1 was generated and compared with the Boltzmann factor $p = \exp(-\Delta E/k_B T)$. The movement was accepted only if $f < p$. If $p \leq f$, the disk was returned to the prior position. The step length s was adjusted so that, on average, about 70% of the attempted moves were accepted: s was increased if the acceptance rate was >85%, decreased if <60%.

Initially, the disks were arranged on a regular lattice. To avoid possible dependence on the initial condition, we monitored an order parameter defined as $O(\mathbf{k}) = (1/N)\ \Sigma_i \cos(\mathbf{k} \cdot \mathbf{r}_i)$, where $\mathbf{k}$ is a reciprocal lattice vector of the initial lattice and $\mathbf{r}_i$ is the position vector of the ith disk ($i = 1, 2, \ldots, N$) (Allen and Tildesley, 1987). We noted that, after a few hundred Monte Carlos steps, $O(\mathbf{k})$ approached the value $1/N$, indicating that the initial lattice had melted (or randomized). Thereafter, the position correlation function $n_{01}(r)$ was constructed from the disk distribution every five steps. The result shown in Fig. 6 is the average of 20,000 Monte Carlo steps. The simulations were repeated with different values of height U_o and range A_1 until the simulated $n_{01}(r)$ agreed with the experimental $n_{01}(r)$. We see that the experimental data can indeed be explained by such a model with an appropriate choice of parameters: $U_o = 2.2k_BT$, and $A_1 = 44$ Å (see Fig. 6). However the fit was not sensitive to the functional form for the potential. For example, the linear potential could be replaced by an exponential potential of the similar height and the similar range, and the result would still fit the data. The definitive conclusion is that the potential is repulsive, of magnitude $\sim 2k_BT$ and of range ~ 40 Å. In comparison, analysis of the gramicidin pattern (Fig. 4, *right*) showed that the interbilayer repulsive potential between gramicidin channels is of magnitude $\sim 4k_BT$ and range ~ 15 Å.

We speculate that such repulsive potentials could originate from the hydration force (Israelachvili, 1992; Rand and Parsegian, 1989). It is well known that two fluid-like amphiphilic surfaces, such as two apposing bilayers, exhibit short-range repulsive forces perpendicular to the surfaces. If the bilayers contains pores, the potential surface associated with the hydration force will not be flat. As a result, the hydration force can cause horizontal repulsion between a pore in one bilayer and another pore in the next bilayer so as to lower the total potential energy. We can understand this by considering an example of electrostatic repulsive force: Two large, parallel plane conductors are kept at a fixed distance. Each plane conductor has a circular hole and both conductors are positively charged. It is easy to show that the electric potential is maximum when the two holes are lined up and have the same in-plane position, and is minimum when the two holes are infinitely separated. Therefore, there is a horizontal (i.e., in-plane) repulsive force between these two holes. Similarly, it is energetically unfavorable to have pores in two neighboring bilayers to have the same in-plane position when there is a hydration force between the two bilayers. This effect is not significant when the samples are fully hydrated because, in this condition, the bilayers are well separated. The hydration force has a range of 10–20 Å and decreases exponentially with a decay length ~1–3 Å (Israelachvili, 1992; Rand and Parsegian, 1989; McIntosh and Simon, 1986). The effect becomes stronger as the separation between bilayers shortens with increasing dehydration. The phenomena of interbilayer correlations observed in the magainin and gramicidin patterns are consistent with this qualitative description.

Case 3: Strong interbilayer correlations

In the experimental paper (Yang et al., 1998), we showed that the liquid-like diffraction pattern of magainin in DMPC/DMPG (3:1) bilayers at 35°C transformed to a crystal-like diffraction pattern when the sample was cooled to below 20°C, while the sample humidity was kept at ~95% RH. We have found that crystallization could also be achieved by dehydration, and similar effects have been observed for magainin in a variety of lipids. Figure 7 shows an example of magainin in DMPC bilayers at various levels of hydration. Both the effects of dehydration and cooling were reversible. So far crystal-like patterns have not been observed in gramicidin or alamethicin samples, however.

We note that both the liquid-like and crystal-like diffraction patterns appear in the range of $|\mathbf{q}| < 0.1$ Å^{-1}, corresponding to structures larger than 60 Å. The only known lipid organization in this range of $|\mathbf{q}|$ is the rippled (P_β) phase (Wack and Webb, 1989), besides the obvious first-order Bragg peaks of lamellar, hexagonal, or cubic phases (Seddon, 1989). The diffraction patterns of various phases of lipids are readily recognizable. Most of the crystal-like diffraction patterns observed in our experiment are clearly distinct from the known lipid patterns. For example, in Fig. 7, the crystal-like diffraction spots developed directly on the liquid-like pattern of magainin pores when (T, RH) was changed from (32°C, 90%) to (28°C, 85%). The discovery of the crystalline phase of peptide organizations in membranes points to the possibility of high-order diffraction of these supramolecular structures, that should be investigated with appropriate diffractometers.

CONCLUSION

We presented here the basic principles for analyzing the off-plane diffraction patterns of oriented membrane multilayers. The structures in fluid membranes are obtained by analyzing the form factor $F_\phi(q_z, q_r)$ and the in-plane structure factor $S_{00}(q_r)$. In particular, with the aid of deuteration contrast variations, one can measure the inside and outside diameters of the membrane pores rather precisely. $S_{00}(q_r)$ can be measured directly by in-plane scattering, provided there are no interbilayer correlations. However, the only way to be certain of no interbilayer correlations in a sample is by measuring its off-plane diffraction and showing that its

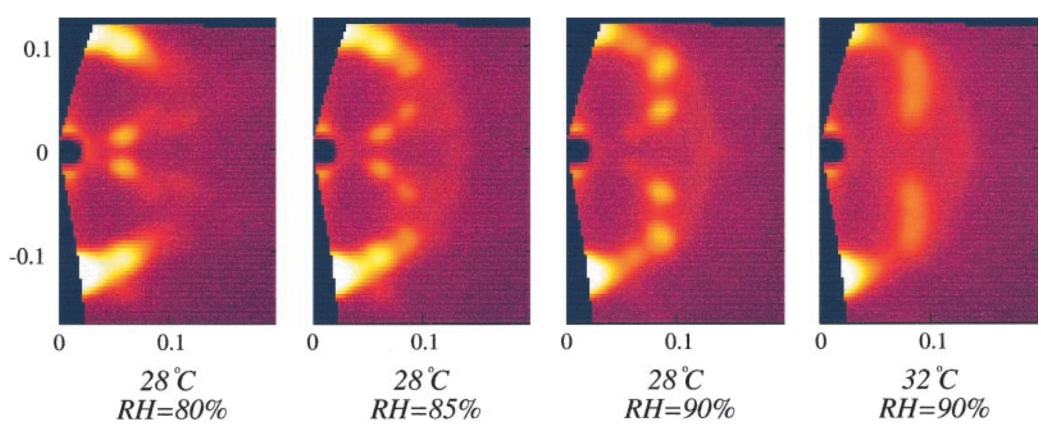

FIGURE 7 Diffraction patterns on (q_z ordinate, q_r abscissa; unit Å^{-1}) of one magainin sample in different temperature and hydration levels. Magainin was in DMPC bilayers at the peptide-to-lipid molar ratio 1/30.

q_z-dependence is the same as that of the form factor squared.

It is a general trend that interbilayer correlations increase with dehydration. But the degree of correlation varies a great deal with both peptide and lipid. Furthermore, at some point of dehydration, the lipid matrix may undergo the fluid-to-gel phase transition that will affect the peptide–lipid interactions. As long as the interbilayer correlations are weak, the diffraction patterns can be analyzed with a truncated expansion of $S(q_z, q_r)$, involving only $S_{00}(q_r)$ and $S_{01}(q_r)$. In the examples we have analyzed, $S_{00}(q_r)$ extracted from the off-plane diffraction pattern measured at ~95% RH is similar to that measured by in-plane scattering at full hydration. $S_{01}(q_r)$ describes a completely new phenomenon that is yet to be explored. Upon further dehydration, the interbilayer correlations sometimes lead to crystallization, from which one can obtain high-order diffraction by the array of supramolecular structures. Potentially, a higher resolution structural analysis can be achieved.

Oriented membrane multilayers are becoming standard samples for x-ray, neutron, and solid state NMR investigations. These samples are extremely sensitive to the degree of hydration. Thus, it is crucial to understand the effect of dehydration when such samples are used. It has been known that dehydration affects the physical state of the lipid matrix (Smith et al., 1990), and the state (e.g., orientation) of peptides in bilayers (Huang and Wu, 1991; Heller et al., 1997, 1998). This study demonstrated that dehydration can also cause correlations of the in-plane positions of peptide pores between adjacent bilayers. In biophysics, one often desires to study the sample in full hydration, so as to relate the results to physiological conditions. However, in the fully hydrated condition, the membrane multilayers are so fluid that the samples are difficult to handle. More importantly, the undulation fluctuations of lipid bilayers in the fully hydrated condition significantly diminish the structural order one wishes to obtain in an oriented sample. Both the fluidity and undulation fluctuations decrease to a manageable level as soon as the sample is dehydrated to a level corresponding to about 98% RH. Thus, in reality, oriented multilayer samples are usually measured in less than fully hydrated conditions. The best method of experiment is to vary the hydration level of the sample as an experimental parameter, and extrapolate the experimental results as a function of hydration to the full hydration limit. For example, we have shown that the bilayer thickness approaches a constant value toward full hydration (Wu et al., 1995; Ludtke et al., 1995; Chen et al., 1997). Thus, it is possible to study the properties of fully hydrated membranes without a direct measurement at full hydration. From this point of view, dehydration is a means of controlling the undulation fluctuations of lipid bilayers. The potential use of hydration/dehydration as an experimental variable is yet to be fully explored. In this study, dehydration led to discoveries of new phenomena, including interbilayer correlations and crystallization of membrane-embedded peptide assemblies.

This work was supported by NIH grant GM55203 and NIH training grant GM08280, and by the Robert A. Welch Foundation. We acknowledge the support of the National Institute of Standards and Technology, U.S. Department of Commerce, in providing the neutron research facilities used in this work, which was also supported by the National Science Foundation under agreement No. DMR-942310.

REFERENCES

Allen, M. P., and D. J. Tildesley. 1987. Computer Simulations of Liquids. Oxford University Press, New York. 118–123.

Arseniev, A. S., V. F. Bystrov, T. V. Ivanov, Y. A. Ovchinnikov. 1985. ^{1}H-NMR study of gramicidin-A transmembrane ion channel. Head-to-head right-handed single stranded helices. *FEBS Lett.* 186:168–174.

Bacon, G. E. 1975. Neutron Diffraction. 3rd ed, Clarendon Press, Oxford, U.K. 544–580.

Baumann, G., and P. Mueller. 1974. A molecular model of membrane excitability. *J. Supramol. Struct.* 2:538–557.

Caillé, A. 1972. Remarques sur la diffusion des rayons X dans les smectiques. *C.R. Acad. Sci. Serie B.* 274:891–893.

Chen, F. Y., W. C. Hung, and H. W. Huang. 1997. Critical swelling of phospholipid bilayers. *Phys. Rev. Lett.* 79:4026–4029.

Duclohier, H., G. Molle, and G. Spach. 1989. Antimicrobial peptide magainin 1 form *Xenopus* skin forms anion permeable channels in planar lipid bilayers. *Biophys. J.* 56:1017–1021.

Dufourcq, J., J.-F. Faucon, G. Fourche, J.-L. Dasseux, M. Le Maire, and T. Gulik-Krzywicki. 1986. Morphological changes of phosphatidylcholine bilayers induced by melittin: vesicularization, fusion, discoidal particles. *Biochim. Biophys. Acta.* 859:33–48.

Fox, R. O., and F. M. Richards. 1982. A voltage-gated ion channel model inferred from the crystal structure of alamethicin at 1.5-Å resolution. *Nature.* 300:325–330.

Hansen, J.-P., and I. R. McDonald. 1986. Theory of Simple Liquids. 2nd ed, Academic Press, New York. 45–68.

Harroun, T. A., W. T. Heller, T. M. Weiss, L. Yang, H. W. Huang. 1999a. Experimental evidence for hydrophobic matching and membrane-mediated interactions in lipid bilayers containing gramicidin. *Biophys. J.* 76:937–945.

Harroun, T. A., W. T. Heller, T. M. Weiss, L. Yang, H. W. Huang. 1999b. Theoretical analysis of hydrophobic matching and membrane-mediated interactions in lipid bilayers containing gramicidin. *Biophys. J.* 76: 3176–3185.

He, K., S. J. Ludtke, Y. Wu, and H. W. Huang. 1993a. X-ray scattering with momentum transfer in the plane of membrane: application to gramicidin organization. *Biophys. J.* 64:157–162.

He, K., S. J. Ludtke, Y. Wu, and H. W. Huang. 1993b. X-ray scattering in the plane of membrane. *J. Phys. France IV.* 3:265–270.

He, K., S. J. Ludtke, D. L. Worcester, and H. W. Huang. 1995. Antimicrobial peptide pores in membranes detected by neutron in-plane scattering. *Biochemistry.* 34:15614–15618.

He, K., S. J. Ludtke, D. L. Worcester, and H. W. Huang. 1996. Neutron Scattering in the Plane of Membrane: Structure of Alamethicin Pores. *Biophys. J.* 70:2659–2666.

Heller, W. T., A. J. Waring, R. I. Lehrer, and H. W. Huang. 1998. Multiple states of β-sheet peptide protegrin in lipid bilayers. *Biochemistry.* 37: 17331–17338.

Heller, W. T., K. He, S. J. Ludtke, T. A. Harroun, and H. W. Huang. 1997. Effect of changing the size of lipid headgroup on peptide insertion into membranes. *Biophys. J.* 73:239–244.

Huang, H. W., and G. A. Olah. 1987. Uniformly oriented gramicidin channels embedded in thick monodomain lecithin multilayers. *Biophys. J.* 51:989–992.

Huang, H. W., and Y. Wu. 1991. Lipid-alamethicin interactions influence alamethicin orientation. *Biophys. J.* 60:1079–1087.

Israelachvili, J. 1992. Intermolecular and Surface Forces. Academic Press, New York. 128–135.

Juretic, D., R. W. Hendler, F. Kamp, W. S. Caughhey, M. Zasloff, and H. V. Westerhoff. 1994. Magainin oligomers reversibly dissipate $\Delta\mu_{H^+}$ in cytochrome oxidase liposomes. *Biochemistry.* 33:4562–4570.

Ladokhin, A. S., M. E. Selsted, and S. H. White. 1997. Sizing membrane pores in lipid vesicles by leakage of co-encapsulated markers: pore formation by melittin. 72:1762–1766.

Latorre, R., and S. Alvarez. 1981. Voltage-dependent channels in planar lipid bilayer membranes. *Physiol. Rev.* 61:77–150.

Ludtke, S., K. He, and H. W. Huang. 1995. Membrane thinning caused by magainin 2. *Biochemistry.* 34:16764–16769.

Ludtke, S. J., K. He, W. T. Heller, T. A. Harroun, L. Yang, and H. W. Huang. 1996. Membrane pores induced by magainin. *Biochemistry.* 35:13723–13728.

Matsuzaki, K., O. Murase, N. Fujii, K. Miyajima. 1996. An antimicrobial peptide, magainin 2, induced rapid flip-flop of phospholipids coupled with pore formation and peptide translocation. *Biochemistry*. 35: 11361–11368.

Matsuzaki, K., S. Yoneyama, and K. Miyajima. 1997. Pore formation and translocation of melittin. *Biophys. J.* 73:831–838.

McIntosh, T. J., and S. A. Simon. 1986. Hydration force and bilayer deformation. *Biochemistry.* 25:4058–4066.

Nicholson, L. K., and T. A. Cross. 1989. Gramicidin cation channel: an experimental determination of the right-handed helix sense and verification of β-type hydrogen bonding. *Biochemistry.* 28:9379–9385.

Olah, G. A., H. W. Huang, W. Liu, and Y. Wu. 1991. Location of ion binding sites in the gramicidin channel by x-ray diffraction. *J. Mol. Biol.* 218:847–858.

Page, D. I., and K. Mika. 1971. The partial structure factors of molten cuporous chloride from neutron diffraction measurements. *J. Phys.* C4: 3034–3044.

Rand, R. P., and V. A. Parsegian. 1989. Hydration forces between phospholipid bilayers. *Biochim. Biophys. Acta.* 988:351–376.

Seddon, J. M. 1989. Structure of the inverted hexagonal (H_{II}) phase, and non-lamellar phase transitions of lipids. *Biochim. Biophys. Acta.* 1031: 1–69.

Smith, G. S., E. B. Sirota, C. R. Safinya, R. J. Plano, and N. A. Clark. 1990. X-ray structural studies of freely suspended ordered hydrated DMPC multimembrane films. *J. Chem. Phys.* 92:4519–4529.

Tosteson, M. T., and Tosteson, C. 1981. The sting. Melittin forms channels in lipid bilayers. *Biophys. J.* 36:109–116.

Wack, D. C., and W. W. Webb. 1989. Synchrotron x-ray study of the modulated lamellar phase $P_{\beta'}$, in the lecithin-water system. *Phys. Rev.* 40A:2712–2730.

Warren, B. E. 1969. X-ray diffraction. Dover, New York. 315–357.

Wu, Y., K. He, S. J. Ludtke, and H. W. Huang. 1995. X-ray diffraction study of lipid bilayer membrane interacting with amphiphilic helical peptides: diphytanoyl phosphatidylcholine with alamethicin at low concentrations. *Biophys. J.* 68:2361–2369.

Yang, L., T. A. Harroun, W. T. Heller, T. M. Weiss, and H. W. Huang. 1998. Neutron off-plane scattering of aligned membranes. I. Method of measurement. *Biophys. J.* 75:641–645.